Exploring Graphene's Impact on Graphite/PANI Matrix Composites: High-Press Fabrication and Enhanced Thermal-Electrical Properties

Murat Ozlek[a], Merve Sehnaz Akbulut[a] and Engin Burgaz[a,b]*

[a] Department of Nanoscience and Nanotechnology, Ondokuz Mayis University, Atakum, 55139, Samsun, Turkey

[b] Department of Metallurgical and Materials Engineering, Ondokuz Mayis University, Atakum, 55139, Samsun, Turkey

* Corresponding Author

*E-mail address: eburgaz@omu.edu.tr

Table S1. Thermal Conductivity Parameters

Sample Name	Width (meter)	Thickness (meter)	(ΔL_1) Distance between probes (Sample)	(ΔL_2) Distance between probes (Cu)	A1 (Cross Section Area of Sample)	A2 (Cross Section Area of Cu)	κ_{Cu} ($W.m^{-}K^{-1}$)	(ΔT_1) Temperature difference on sample	(ΔT_2) Temperature difference on Cu	Thermal Conductivity ($W.m^{-1}K^{-1}$)
GP	0.006	0.002	0.007	0.014	0.000012	0.000035	400	4.5	2	259.25
GGP-7	0.0055	0.00095	0.006	0.009	0.000005225	0.000035	400	12.5	2.6	371.54
GGP-10	0.007	0.00056	0.005	0.014	0.00000392	0.000035	400	16	3.6	286.98
GGP-14	0.004	0.00151	0.007	0.009	0.00000604	0.000035	400	12.2	3.4	502.41
GGP-17	0.007	0.00145	0.006	0.009	0.00001015	0.000035	400	8.1	3.6	408.68
GGP-21	0.008	0.00069	0.007	0.014	0.00000552	0.000035	400	7.4	3.6	616.92
GP 527 MPa	0.0075	0.00029	0.0075	0.009	0.000002175	0.000035	400	14.2	2.8	1057.68
GGP-7 527 MPa	0.009	0.00021	0.0075	0.009	0.00000189	0.000035	400	12.5	3.1	1530.86
GGP-10 527 MPa	0.005	0.00019	0.008	0.009	0.00000095	0.000035	400	20.5	2.8	1789.18
GGP-14 527 MPa	0.0035	0.00023	0.008	0.013	0.000000805	0.000035	400	13.3	2.8	2253.12
GGP-17 527 MPa	0.007	0.00021	0.0075	0.009	0.00000147	0.000035	400	14.2	2.6	1453.16
GGP-21 527 MPa	0.005	0.00019	0.0075	0.009	0.00000095	0.000035	400	17.2	2.4	1713.58

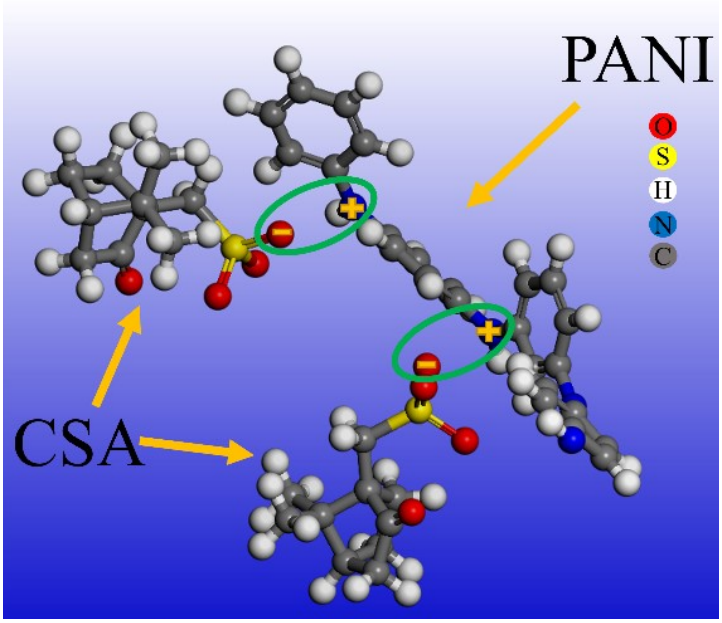

Figure S1. The protonation of PANI repeating units with camphor-sulfonic acid

Table S2. Binding energy and area values of XPS results for GP 527 MPa and GGP-14 527 MPa samples

Sample	XPS Peaks	Peak Name	e Value	Area (%)	Bond Name
GP 527 MPa	C1s	A	283.28	3.415	C-C
	C1s	B	284.5	69.280	C=C
	C1s	C	285.58	9.632	C-N
	C1s	D	286.64	6.277	C-H
	C1s	E	288.88	2.768	C-O
	O1s	A	531.95	3.947	O-H
	O1s	B	533.42	3.986	O=C
	O1s	-	-	-	O-N
	N1s	A	399.53	0.690	N-H
	N1s	-	-	-	N-C
	N1s	-	-	-	N=O
GGP-14 527 MPa	C1s	A	283.36	3.464	C-C
	C1s	B	284.5	53.867	C=C
	C1s	C	285.52	11.35	C-N
	C1s	D	286.7	7.065	C-H
	C1s	E	288.78	2.352	C-O
	O1s	A	531.04	6.614	O-H
	O1s	B	531.98	7.175	O=C
	O1s	C	533.37	4.413	O-N
	N1s	A	399.15	1.924	N-H
	N1s	B	400.23	1.258	N-C
	N1s	C	401.74	0.513	N=O

UV-Vis spectroscopy was utilized to analyze the optical properties of GGP samples as shown in Figure S2. The measurements were performed using an Agilent Cary 60 UV-Vis spectrophotometer. The scan was carried out from 200 nm to 650 nm to capture both the ultraviolet and visible regions. The data was collected with a scan rate of 24,000 nm/min and a data interval of 5.0 nm, providing a high-resolution absorption spectrum. The UV-Vis absorption spectra for the GGP samples (GGP7, GGP10, GGP14, and GGP21) are presented in Figure S2. Each sample exhibits a strong absorption peak in the 200-250 nm range, which corresponds to π-π *transitions** in the

conjugated systems of carbon-carbon double bonds (C=C). These transitions are characteristic of the electronic excitations within the conjugated aromatic systems, such as those found in polyaniline (PANI) and graphene present in the GGP composites. As the graphene content approaches 14 wt.%, there is a notable sharpening of the absorption peak, particularly in the GGP14 sample. This sharpening suggests more defined π-π* transitions due to enhanced conjugation in the composite (1,2). The increased graphene content likely leads to better π-π stacking interactions, improving the alignment and electronic delocalization in the material until 21 wt.% graphene content. This trend can be observed when comparing the spectra, where the GGP14 sample displays a sharper and more intense peak in the 230 nm region, indicating stronger π-π* transitions compared to the other samples. The shoulder observed in the region between 400-600 nm suggests the presence of polaronic transitions, likely a result of the interactions between the polyaniline and graphene/graphite components. These interactions are known to facilitate charge transfer, enhancing the optical and electronic properties of the composites.

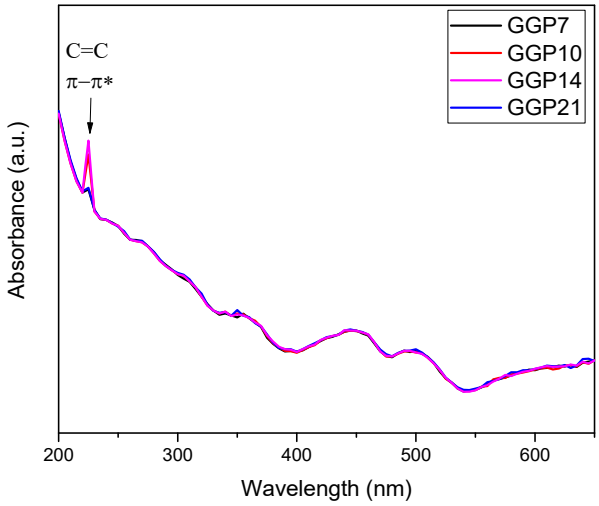

Figure S2.UV-vis spectra of GGP samples.

The carrier concentration and mobility measurements in Figure S3 were done by using Ecopia HMS 3000 Hall Effect Measurement System. The measurement parameters were set to a current value of 0.5 mA and a magnetic field strength of 0.55 T. The carrier concentration and mobility data for GP, GGP-7, GGP-10, GGP-14, and GGP-21 pressed samples reveal important trends in charge carrier dynamics with varying graphene content. GP typically exhibit higher carrier concentration due to the abundance of charge carriers in graphite layers. However, their contribution to carrier mobility is limited because electron scattering occurs at grain boundaries, vacancies and dislocations within the graphite structure. As the graphene ratio in GGP samples increases, the carrier concentration decreases compared to GP samples, but the carrier mobility increases. This is because graphene sheets offer low-resistance pathways for electron flow due to their two-dimensional structure and exceptional electrical conductivity, in contrast to the high-resistance locations of large graphite structures. When the graphene ratio reaches 14 wt.%, the carrier concentration drops to the lowest value among samples. However, the electrons contribute more effectively to electrical conductivity, as evidenced by a carrier mobility of 248 $cm^2V^{-1}s^{-1}$. This indicates that electrons are predominantly flowing through interconnected graphene networks, which provide efficient conduction paths. In GGP-21 527 MPa sample, carrier concentrations start to increase again, but the carrier mobility dramatically decreases. This may be due to excessive graphene content leading to restacking or aggregation of graphene layers, creating high-resistance regions that impede electron flow. According to XRD and Raman analyses, the interlocking of graphene between large graphite structures increases the interlayer distance of graphite layers and introduces defects in GGP-14 527 MPa sample. These changes create opportunities for better electron flow by providing low-resistance defect locations, thereby increasing electrical conductivity.

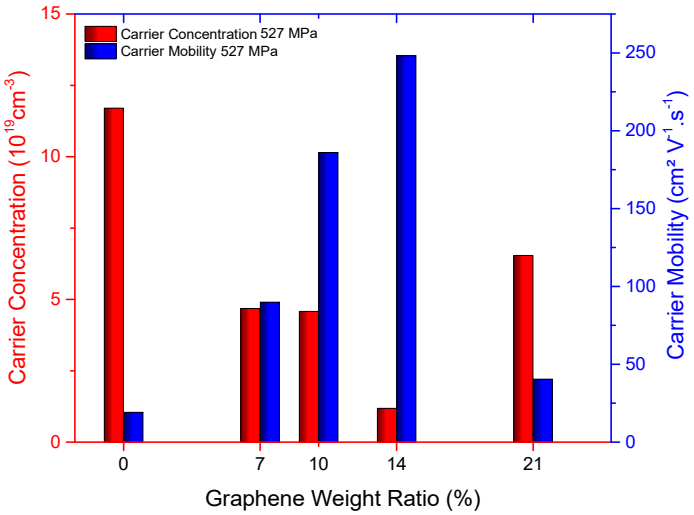

Figure S3. Carrier concentration and mobility of pressed GP and GGP samples

References

1. Zhang J, Yang H, Shen G, Cheng P, Zhang J, Guo S. Reduction of graphene oxide via L-ascorbic acid._Supporting Information. Chem Commun (Camb). 2010;2(c).

2. Johra FT, Lee JW, Jung WG. Facile and safe graphene preparation on solution based platform. J Ind Eng Chem [Internet]. 2014;20(5):2883–7. Available from: http://dx.doi.org/10.1016/j.jiec.2013.11.022